



# Granulosa cells provide elimination of apoptotic oocytes through unconventional autophagy-assisted phagocytosis

M.G. Yefimova, C Lefevre, Anu Bashamboo, C Eozenou, A Burel, M. T. Lavault, Ac Meunier, C Pimentel, S Veau, A. S. Neyroud, et al.

## ► To cite this version:

M.G. Yefimova, C Lefevre, Anu Bashamboo, C Eozenou, A Burel, et al.. Granulosa cells provide elimination of apoptotic oocytes through unconventional autophagy-assisted phagocytosis. Human Reproduction, 2020, 35 (6), pp.1346-1362. 10.1093/humrep/deaa097 . hal-02888701

**HAL Id: hal-02888701**

**<https://hal.science/hal-02888701>**

Submitted on 10 Jul 2020

**HAL** is a multi-disciplinary open access archive for the deposit and dissemination of scientific research documents, whether they are published or not. The documents may come from teaching and research institutions in France or abroad, or from public or private research centers.

L'archive ouverte pluridisciplinaire **HAL**, est destinée au dépôt et à la diffusion de documents scientifiques de niveau recherche, publiés ou non, émanant des établissements d'enseignement et de recherche français ou étrangers, des laboratoires publics ou privés.

**Granulosa cells provide elimination of apoptotic oocytes through unconventional autophagy-assisted phagocytosis**

M.G. Yefimova<sup>1,2\*</sup>, C. Lefevre<sup>3</sup>, A. Bashamboo<sup>4</sup>, C. Eozenou<sup>4</sup>, A. Burel<sup>5</sup>, M.T. Lavault<sup>5</sup>, A.C. Meunier<sup>6</sup>, C. Pimentel<sup>1</sup>, S. Veau<sup>1</sup>, A.S. Neyroud<sup>1</sup>, S. Jaillard<sup>1</sup>, B. Jégou<sup>3</sup>, N. Bourmeyster<sup>6,7</sup>, C. Ravel<sup>1,3</sup>.

<sup>1</sup>Département de gynécologie obstétrique et reproduction humaine - CECOS, CHU de Rennes, 16, boulevard de Bulgarie, 35000 Rennes, France

<sup>2</sup>Sechenov institute of evolutionary physiology and biochemistry, Russian academy of sciences, 44, M. Thorez pr., St-Petersburg 194223, Russia

<sup>3</sup>Univ Rennes, Inserm, EHESP, Irset (Institut de recherche en santé, environnement et travail) - UMR\_S 1085, F-35000 Rennes, France

<sup>4</sup>Human Developmental Genetics, Institut Pasteur, 25-28 Rue du Docteur Roux, Paris 75724, France.

<sup>5</sup>MRic TEM Plateform, BIOSIT, Université Rennes 1, 2, avenue du Pr Léon-Bernard, 35000 Rennes, France.

<sup>6</sup>Laboratoire STIM, Université de Poitiers, 1, rue Georges-Bonnet, 86022 Poitiers cedex, France.

<sup>7</sup>CHU de Poitiers, 2 Rue de la Milétrie, 86021 Poitiers cedex, France

**Corresponding author:** Marina G. Yefimova\*; E-mail: yefimova3@gmail.com

**Running title:** Granulosa cells ingest and destroy the apoptotic oocytes

## 25    **Abstract**

26    **STUDY QUESTION:** Do human granulosa cells (GC) ingest and destroy apoptotic oocytes?

27    **SUMMARY ANSWER:** Somatic GC ingest and destroy apoptotic oocytes and other apoptotic  
28    substrates through unconventional autophagy-assisted phagocytosis.

29    **WHAT IS KNOWN ALREADY:** Most (99%) ovarian germ cells undergo apoptosis through  
30    follicular atresia. The mode of cleaning of atretic follicles from the ovary is unclear. Ovarian GC  
31    share striking similarities with testicular Sertoli cells with respect to their origin and function.  
32    Somatic Sertoli cells are responsible for the elimination of apoptotic spermatogenic cells through  
33    unconventional autophagy-assisted phagocytosis.

34    **STUDY DESIGN, SIZE, DURATION:** Human GC were tested for the ability to ingest and  
35    destroy the apoptotic oocytes and other apoptotic substrates. A systemic study of the main  
36    phagocytosis steps has been performed at different time points after loading of apoptotic  
37    substrates into the GC.

38    **PARTICIPANTS/MATERIALS, SETTING, METHODS:** Primary cultures of GC retrieved  
39    following controlled ovarian stimulation of five women for IVF/ICSI and a human granulosa  
40    KGN cell line were incubated with different apoptotic substrates: oocytes which underwent  
41    spontaneous apoptosis during the cultivation of immature germ cells for IVF/ICSI; apoptotic  
42    KGN cells; and apoptotic membranes from rat retinas. Cultured GC were analyzed for the  
43    presence of specific molecular markers characteristic of different steps of phagocytic and  
44    autophagy machineries by immunocytochemistry, confocal microscopy, transmission electron  
45    microscopy and western blotting, before and after loading with apoptotic substrates.

46    **MAIN RESULTS AND THE ROLE OF CHANCE:** Incubation of human GC with apoptotic  
47    substrates resulted in their translocation in cell cytoplasm, concomitant with activation of the  
48    phagocytosis receptor c-mer proto-oncogene tyrosine kinase MERTK ( $P<0.001$ ), clumping of

motor molecule myosin II, recruitment of autophagy proteins: autophagy related protein 5 (ATG5), autophagy-related protein 6 (Beclin1) and the rise of a membrane form of microtubule-associated protein 1 light chain 3 (LC3-II) protein. Ingestion of apoptotic substrates was accompanied by increased expression of the lysosomal protease Cathepsin D ( $P < 0.001$ ), and a rise of lysosomes in the granulosa cells, as assessed by different techniques. The level of autophagy adaptor, sequestosome 1/p62 (p62) protein remained unchanged.

**LARGE SCALE DATA:** N/A

**LIMITATIONS, REASONS FOR CAUTION:** The number of patients described here is limited. Also the dependence of phagocytosis on reproductive hormone status of patients should be analyzed.

**WIDER IMPLICATIONS OF THE FINDINGS:** Removal of apoptotic oocytes by surrounding GC seems likely to be a physiological mechanism involved in follicular atresia. Proper functioning of this mechanism may be a new strategy for the treatment of ovarian dysfunctions associated with an imbalance in content of germ cells in the ovaries, such as premature ovarian failure and polycystic ovary syndrome.

**STUDY FUNDING/COMPETING INTEREST(S):** The study was funded by Rennes Metropole (AIS 2015) and Agence de BioMédecine. This work was supported by funding from Université de Rennes1, Institut National de la Santé et de la Recherche Médicale (INSERM) and CHU de Rennes. A. Bashamboo is funded in part by the program Actions Concertées Interpasteuriennes (ACIP) and a research grant from the European Society of Pediatric Endocrinology. This work is supported by the Agence Nationale de la Recherche Grants ANR-17-CE14-0038 and ANR-10-LABX-73. The authors declare no competing interests.

**TRIAL REGISTRATION NUMBER:** GMR 2017-03

72 **Key words:** granulosa cells/apoptotic oocytes/follicular atresia/phagocytosis/autophagy/LC3-  
73 associated phagocytosis/ Sertoli cells/photoreceptor outer segments/premature ovarian  
74 failure/polycystic ovary syndrome

75

## 76 **Introduction**

77 Apoptosis is a vital process that occurs in normal and pathological conditions in all  
78 tissues of the body (Elmore, 2007). Once formed, apoptotic cells are immediately eliminated by  
79 cells endowed with phagocytic activity. Phagocytosis of apoptotic cells or cell debris is a  
80 complex receptor-mediated process. The coordinated action of membrane-bound receptors  
81 triggers signaling mechanisms, which stimulate the ingestion of apoptotic substrates for their  
82 further degradation by lysosomal enzymes (Yefimova et al., 2018). Using specific receptors,  
83 phagocytes recognize and bind to the specific “eat-me” signals appearing on apoptotic cell  
84 surfaces, such as externalized phosphatidylserine (PS) (Wu et al., 2006). Both the timely and  
85 complete clearance of apoptotic substrates is important to maintain tissue homeostasis, and to  
86 avoid the autoimmune response against intracellular antigens (Itoh et al., 1999).

87 The mammalian ovary is an extremely dynamic organ, in which 99 % of ovarian germ  
88 cells undergo apoptosis through follicular atresia (Matsuda et al., 2012). Atresia can affect the  
89 follicles at all stages of their development, so that both oocytes and surrounding granulosa cells  
90 (GC) go through cell death. The pattern of atresia depends on the phase of follicular maturation.  
91 Thus, in primordial, primary and small pre-antral follicles apoptotic cell death affects oocytes,  
92 while in late pre-antral, antral and ovulatory follicles, apoptosis triggers granulosa cell death  
93 (reviewed by Yadav et al., 2018). The mode of removal of the atretic follicles from the ovary  
94 remains unknown (Yadav et al., 2018). Indeed, the blood-follicular barrier protects ovarian tissue  
95 from blood-circulating phagocytes (Siu & Cheng, 2012). Besides, resident ovarian macrophages  
96 exhibit a very limited ability to phagocytose the extrinsic substrates (Itoh et al., 1999). The role

of these immune cells is mainly related to folliculogenesis regulation, but not to phagocytic function (Katabushi et al, 1996; Gaytán et al., 1998; Wu et al., 2004; Ono et al., 2018).

Massive cell death also occurs in the male reproductive system, wherein 75% of spermatogenic cells undergo apoptosis in blood-separated seminiferous tubules (Shaha et al., 2010). Removal of apoptotic substrates is carried out by the somatic Sertoli cells (Jégou, 1993; Yefimova et al., 2018), which share striking similarities with ovarian GC with respect to their origin and function (Mork et al., 2012). Phagocytic elimination of apoptotic substrates by the Sertoli cells proceeds through LC3-associated phagocytosis (LAP), a hybrid process in which the phagocytic machinery is supported by autophagy degradation (Sanjuan et al., 2007; Yefimova et al., 2013; Panneerdoss et al., 2017).

In contrast to phagocytosis, which provides the degradation of extracellular substrates, autophagy is a lysosome-dependent degradation pathway, which destroys the different substrates of intracellular origin (Mizushima et al., 2008; Yin et al., 2016). Autophagy can be initiated by different stimuli, including nutrient deprivation, metabolic and infection-mediated stresses, cancer, neurodegeneration, and others. Autophagy is regulated by the autophagy-related (*ATG*) genes, which were originally identified in yeast, and their mammalian homologs (Mizushima et al., 2011). Before degradation within the lysosome, substrates to be eliminated are enclosed in an autophagosome, which is a double membrane-limited vacuole containing a lipidated form of LC3 protein (*ATG8*): the latter is currently used as a molecular marker to monitor autophagy (Klionsky et al., 2016).

Exploitation the autophagy component by phagocytosis machinery increases its efficiency, providing rapid lysosomal fusion and cargo degradation (Heckmann et al., 2017). The term LAPosome was proposed to define the particular structure, which harbors the substrate for degradation by LAP. In contrast to an autophagic vacuole, the LAPosome is a single-membrane vesicle coated with lipidated LC3 protein. The presence of LC3 protein distinguishes a LAPosome from the single-membrane phagosome vesicle (Heckmann et al., 2017). LAP-specific

genes include *ATG5*, autophagy-related gene 7 (*ATG7*), *Beclin1*, *Rubicon* (RUN domain and cysteine-rich domain containing Beclin 1-interacting protein) and *NOX2* (NADPH oxidase-2) (Bandyopadhyay & Overholtzer, 2016). While using several autophagy proteins, LAP is independent of the autophagy preinitiation complex (ATG13-ULK1 (Unc-51 like autophagy activating kinase 1)-RB1CC1/FIP200 (RB1 inducible coiled-coil 1)-ATG101) (Kim et al., 2013; Martinez et al., 2015; Masud et al., 2019). In macrophages and in retinal pigmented epithelial cells, autophagy components *ATG5*, *ATG7*, *ATG3*, *ATG12*, *ATG16L1* and a *Beclin1*-*PIK3C3* (Phosphatidylinositol 3-Kinase Catalytic Subunit Type 3)/*VPS34* (vacuolar protein sorting) complex lacking *ATG14* are engaged in the lipidation of *LC3* protein and its recruitment to the phagosome. LAP also requires *Rubicon* for proper function (Martinez et al., 2015; Muniz-Feliciano et al., 2017). *Beclin1*, *ATG5* and *Rubicon* proteins have been detected in LAPosomes from different types of phagocytic cells (blood macrophages, retinal pigmented epithelial cells) that use LAP (Amer & Swanson, 2005; Martinez et al., 2011; Wirawan et al., 2012; Kim et al., 2013; Martinez et al., 2015).

The phagocytic ability of GC *in situ* has been noticed by numerous investigators, who observed ingested material in the cytoplasm of GC at all stages of follicular development (cited from Kasuya, 1997; Gaytan et al., 1998). Living GC eliminate their apoptotic counterparts produced during follicular atresia (Kasuya, 1997; Gaytán et al., 1998). GC from atretic follicles show an activation of autophagy (Yadav et al., 2018) and increased expression of the phagocytosis receptor *MERTK* (Hatzirodos et al., 2014), which is the main receptor mediating the ingestion of apoptotic substrates during LAP (Kim et al., 2013; Yefimova et al., 2013; Panneerdoss et al., 2017). These data suggest the involvement of both phagocytosis and the autophagy degradation machinery in the process of follicular atresia.

Paradoxically, a possible involvement of GC in the elimination of apoptotic germ cells/oocytes has never been considered. In this work, we aimed to test the ability of GC to ingest and destroy the apoptotic oocytes as well as other apoptotic substrates, and to get insights into

molecular mechanisms of this process. Using the human granulosa cell line KGN and primary cultures of human GC, we undertook a systemic study of the main steps involved in the ingestion and degradation of apoptotic substrates, using cytochemistry, immunocytochemistry, electron microscopy and western blotting (WB). In our *in vitro* study we show for the first time that GC efficiently phagocytose apoptotic oocytes as well as other apoptotic substrates. Intracellular management of ingested substrates is facilitated by autophagy degradation machinery through a process strongly resembling LAP, which is responsible for the degradation of apoptotic germ cells by the somatic Sertoli cells from the testis.

## **Materials and Methods**

### **Cells, cell cultures and animals**

#### *Primary culture of human GC*

GC samples were provided by the BioBankGermetheque (BBMRI, France). Fresh GC were retrieved following controlled ovarian stimulation for IVF/ICSI from five patients submitted to standard protocols (Jungheim et al., 2015). All patients signed an informed consent. GCs were isolated from corona radiata and a part of the cumulus oophorus. This suspension was enzymatically treated using 80 IU Hyaluronidase (HYA001; FertiPro NV, Belgium) to separate oocytes from GCs. Oocytes were evacuated with a glass capillary and afterwards, inactivation medium was added into the GCs suspension. GCs inactivation medium consisted of M199 medium (M3769; Sigma, St. Louis, MO, USA), supplemented with 20% fetal calf serum (FCS, 12133C; Sigma, St. Louis, MO, USA) and 1% antibiotic mix (10 000 U/ml penicillin and 50 mg/ml streptomycin, 15140; Gibco Waltham, MA, USA). GCs suspension was centrifuged at 450g for 10 min at 20°C, and then the pelleted cells were suspended in supplemented M199 medium (see above) and seeded in the 5-well culture dish for denudation (16004; Vitrolife, Sweden).



### *Human apoptotic oocytes*

During the cultivation of immature oocytes, some of them undergo a spontaneous apoptosis (Wu et al., 2000). Oocytes exhibiting morphologic features of apoptosis, such as shrinkage, cytoplasmic condensation, membrane blebbing, and/or nuclear fragmentation (Kerr et al., 1972), were collected and stored at  $-195^{\circ}\text{C}$  before being used as a substrate for phagocytosis studies.

Human granulosa KGN cells were from Pasteur's Institute (Paris, France); human telomerase-immortalized retinal pigment epithelium hTERT-RPE1 cells were from Clontech (C4000-1; Mountain View, CA, USA). KGN GC were cultured in DMEM/F12 medium (31331; Gibco, Waltham, MA, USA), containing 10% FCS (12133C; Sigma, St. Louis, MO, USA) and supplemented with 1% antibiotic mix (15140; Gibco, Waltham, MA, USA). hTERT-RPE1 cells were cultured in DMEM/F12 medium (31330; Gibco, Waltham, MA, USA), supplemented with 10% FCS (12133C; Sigma, St. Louis, MO, USA) and 1% antibiotic mix (as above). For immunocytochemistry experiments  $1.5 \times 10^5$  of KGN or RPE-1 cells were seeded in 8-well Labtek chamber slides (177402; Thermofisher, Waltham, MA, USA) pre-coated with the Fibronectin (F1141; Sigma, St. Louis, MO, USA) according to the manufacturer's protocol. For WB, experiments  $5 \times 10^5$  cells were plated into 6-well dishes and cultured at  $37^{\circ}\text{C}$  with 5%  $\text{CO}_2$ . All cell lines were tested for mycoplasma contamination using mycoplasma detection kit (MycoAlert LT07; LONZA, Basel, Switzerland).

Male Wistar rats, aged 2 months, were obtained from Janvier Labs (RjHan: WI; France).

### Pharmacological reagents and antibodies

Dulbecco's PBS (D5652), bovine serum albumin (BSA) (A9647), ceramide (22244), lead(II) nitrate (228621), ammonium sulfide solution (A1952), rapamycin (R8781),  $\beta$ -glycerophosphate (G-9422), fluorescein isothiocyanate (FITC) (F7250) and 1  $\mu\text{m}$  diameter

carboxylate-modified polystyrene fluorescent beads (L4530) were from Sigma-Aldrich (St. Louis, MO, USA). Polyclonal rabbit primary antibodies anti-ATG5 (NB110-53818), anti-Beclin1 (NB500-249), anti-LC3B (NB100-2220), anti-p62/SQSTM1 (NBP1-48320), anti-zona pellucida glycoprotein 3 (ZP3) (NBP2-30830) and anti-phospho-MERTK (NB300-690) from Novus Biologicals Centennial, CO, USA, and polyclonal goat primary antibody anti-Cathepsin D (sc-6486) was from Santa-Cruz Biotechnology, Santa Cruz, CA, USA. The monoclonal mouse antibodies used were anti-rhodopsin (1D4) (sc-57432; Santa-Cruz Biotechnology, Santa Cruz, CA, USA,) anti-myosin heavy chain antibody (3-48) (NB300-284; Novus Biologicals Centennial, CO, USA), anti-ATG7 (sc-376212; Santa-Cruz Biotechnology, Santa Cruz, CA USA) and anti-GAPDH (sc-47724; Santa-Cruz Biotechnology, Santa Cruz, CA USA). The other antibodies conjugated to horse-radish peroxidase were: secondary anti-rabbit (NA934; GE Healthcare, Chicago, IL, USA), anti-mouse (NA931; GE Healthcare, Chicago, IL, USA) and anti-goat (sc-2020; Santa Cruz Biotechnology, Santa Cruz, CA, USA); for immunostaining: anti-rabbit, anti-mouse, and anti-goat antibodies conjugated to Alexa-488 (CAR-A21441), to Alexa-555 (GAM-A21422, DAM-A31570) from Molecular Probes (Invitrogen; Carlsbad, CA, USA) or to FP-647 (GAR-FPGARBTTG0642) from Interchim (Montflucon, France).

#### Isolation of photoreceptor outer segments

Photoreceptor outer segments (POS) have externalized PS on their outer membrane leaflet, therefore are currently used as apoptotic-like substrate for phagocytosis studies (Finnemann et al., 1997; Yefimova et al., 2013).

POS were isolated from the eyes of 2-month-old Wistar rats as described earlier (Yefimova et al., 2013). Briefly, the rats were euthanized with CO<sub>2</sub>. Freshly enucleated eyes were dissected, the retinae were removed from the eyecups and suspended in 0.3M Mannitol/PBS solution, pH 7.4 (0°C), containing 1% antibiotic mix (10 000 U/ml penicillin and 50 mg/ml streptomycin, 15140; Gibco, Waltham, MA, USA), and then vortexed for 20-60 sec

and allowed to stand until the retinae settled. The supernatant containing the POS was collected, centrifuged at 10 000 g for 15 min. To eliminate the traces of mannitol, the pellet containing POS was washed twice with PBS medium supplemented with antibiotic mix (see above). Before the second centrifugation, the suspension of POS was aliquoted in 1.5 ml Eppendorf tubes and centrifuged again. After removing the supernatant, the aliquoted POS were stored in “dry” form at -80°C before use. Each tube contained the POS from one retina.

#### Ceramide treatment

To induce apoptosis, cultured KGN cells were exposed to 10 µm exogenous ceramide for 24h (Davis et al., 2000). The next day the cells were scraped from 6-well dishes, counted, and used as a phagocytosis substrate.

#### FITC labeling for immunofluorescence analysis

For immunofluorescence (IF) analysis, phagocytosis substrates (apoptotic oocytes, apoptotic KGN cells, POS) were labeled using 1mg/ml FITC in 0.1M Na-bicarbonate (pH 9.0) for 1h at 4°C in the dark, then washed and suspended in PBS.

#### Phagocytosis experiments

24h after the seeding of primary human GC, KGN and hTERT-RPE1 cells, the culture media was replaced. The fresh culture media was the same, except that the content of FCS was reduced to 2% in order to slow cell growth during experiments, and to minimize the modulatory effect of serum on phagocytosis rate (Johnston et al., 1969). All phagocytosis substrates as POS, apoptotic oocytes, apoptotic granulosa cells (labeled or unlabeled with FITC) or carboxylate-modified polystyrene fluorescent beads (used as a control) were added to cells at a ratio 10/1. The time of incubation of cells with phagocytosis substrates ranged from 0 to 24 hrs. At the end

of the incubation, the cells were washed from unbound substrates with ice-cold PBS, and then processed for immunocytochemistry or WB experiments.

#### Phagocytosis assay in rapamycin-treated cells

The KGN cells cultured in 8-well Labteck slides (see above) were incubated with 200 nM rapamycin for 24 h, and the culture media was then replaced (as above) and the cells were challenged with POS. At different time points from 0 to 2h, the cells were washed with ice-cold PBS, fixed with 4% paraformaldehyde/PBS (pH 7.4), and then processed for the phagocytosis test, allowing discrimination between bound and ingested substrates (Yefimova et al., 2008; Yefimova et al., 2018). Briefly, the samples were divided into two groups, each in duplicate wells. Group 1 was permeabilized with 0.5% Triton X-100 for 1 min, and group 2 remained unpermeabilized. Then the cells were processed through immunofluorescence using anti-rhodopsin antibody, as described below. The amount of total POS (plasma membrane bound and ingested) was obtained from group 1, and the amount of plasma membrane-bound POS was obtained from group 2. The amount of ingested POS was obtained by subtracting plasma membrane bound POS from total POS. The phagocytosis index was calculated as the ratio of POS area/nuclei area using Image J software (NIH, Bethesda, MD, USA).

#### Western blotting

Proteins were isolated from cell extracts obtained after lysis of  $10^7$  KGN or hTERT-RPE1 cells growing in 6-well dishes. Cells were washed with cold PBS, then collected by scraping on ice in lysis buffer (50  $\mu$ l/per well) containing 50 mM Tris-HCl, 150 mM NaCl, 1 mM EDTA, 1% Triton X-100, phosphatase inhibitor cocktail (04906845001; Roche, Basel, Switzerland) and protease inhibitor cocktail (11697498001; Roche, Basel, Switzerland). Then 4X Laemmli sample buffer was added, and the samples were incubated at 99°C for 10 min. Proteins were separated by electrophoresis on 12% sodium dodecyl-sulphate (SDS)-polyacrylamide gels, then transferred

(2 h, 150 V) to nitrocellulose membranes (0.2  $\mu$ m pore) (GE10600001; Amersham, Buckinghamshire, UK). Blots were blocked for 2 h in TBS containing 5% (w/v) non-fat dry milk. Blots were incubated with anti-phospho-MERTK (1/1000), anti-Beclin1 (1/1000), anti-ATG5 (1/1000), anti-ATG-7 (1/500), anti-LC3 (1/1000), anti-Cathepsin D (1/1000) or anti-GAPDH (1/1000) antibodies in TBS containing 0.5% (w/v) non-fat dry milk at 4°C overnight. Membranes were then incubated with peroxidase-conjugated anti-rabbit (1/10000), anti-mouse (1/10000) or anti-goat (1/5000) antibody in blocking buffer for 1 h at room temperature. Immunodetection was performed with the chemiluminescence substrate Luminata (WBLUF0500; Millipore, Burlington, MA, USA). In some cases, the blots were stripped in 25 mM Glycine-HCl buffer, containing 1% w/v SDS, pH 2 for 30 min; membranes were then washed with TBS, blocked and re-probed as above. Densitometry analysis of specific bands on the blots was performed using ImageJ (NIH, Bethesda, MD, USA) software. In phagocytosis kinetic experiments the blots were normalized to time 0 (cells + phagocytosis substrate at the time 0) to avoid the misinterpretation of the data due to the activation of degradation processes during phagocytosis (see below).

#### Immunocytochemistry

Indirect immunofluorescence was performed following conventional procedures. Briefly, cells growing on 8-well glass Labteck chamber slides were fixed in paraformaldehyde/PBS (pH 7.4), permeabilized with 0.5% Triton X-100/PBS, and then incubated overnight at 4°C with primary antibodies diluted at a ratio 1:250 in 1% BSA/PBS. The dilution of the secondary antibodies was 1:500 in 1% BSA/PBS. Cell nuclei were stained with DAPI (4', 6 diamidino-2-phenylindole; 0.5  $\mu$ g/ml) (62247, Thermo Fisher Scientific, Waltham, MA, USA). Slides were observed under an inverted microscope: DMT 6000 Leica (Leica Microsystems; Wetzlar, Germany). The pictures were taken using a DFC350FX camera (Leica Microsystems; Wetzlar, Germany).

### Cytochemical analysis for lysosomes

In cytochemical experiments a modified Gomori protocol for lysosomal enzyme acid phosphatase was used to stain the lysosomes in the GC (Allison & Mallucci, 1965). Gomori reagent was prepared as follows: 660 mg of lead nitrate was dissolved in 50 ml of 2% solution of  $\beta$ -glycerophosphate in 0.05M sodium-acetate buffer pH 5.0. The mixture was immediately filtered through Whatman Filter paper.

KGN cells cultured on the 1-well glass Labteck slides were challenged with apoptotic substrates. After incubation, the cells were washed in ice-cold PBS and fixed by immersion in -20°C acetone for 40 min. Then the slides were air-dried and incubated in Gomori reagent at 37°C for 6 h. After that the samples were washed in distilled water and immersed in ammonium sulfide solution for 1 min. After washing in distilled water the slides were air-dried and analyzed in Nanozoomer 2.0RS (Hamamatsu, Shizuoka, Japan) using NDP.view2 U12388-21 software (version 2.7, Hamamatsu, Photonics, Japan). In each sample, the brown-stained area corresponding to acid phosphatase was assessed by Image J software and assessed relative to the number of nuclei in the sample.

### Confocal microscopy

Samples were examined by confocal laser scanning microscopy using a confocal FV-1000 station installed on an inverted microscope IX-81 (Olympus, France). Multiple fluorescence signals were acquired sequentially to avoid crosstalk between image channels. Fluorophores were excited with a 405 nm diode (for DAPI), 488 nm line of an argon laser (for AF488), 543 nm line of a He-Ne laser (for AF555), and 633 nm line of a He-Ne laser (for AF647 and FP647). The emitted fluorescence was detected through spectral detection channels in the range 425–475 nm, 500–530 nm, 555–655 nm and >680 nm for blue, green, red and far red fluorescence, respectively. Maximal resolution was obtained with an Olympus UplanSapox60

oil, 1.4 NA, objective lens (Olympus). When necessary, optical sectioning of the specimen (Z series) was driven by a Z-axis stepping motor through the entire thickness of the cell layer. Analysis of confocal images, co-localization studies evaluated with Pearson's correlation coefficient, and modeling of 3D reconstruction images were performed with Imaris 3D (7.2.1) software (Bitplane; Zurich, Switzerland).

#### Transmission electron microscopy

For transmission electron microscopy (TEM), KGN cells were fixed in 2.5% glutaraldehyde (16220; Electron Microscopy Sciences, Hatfield, PA, USA)/0.1M cacodylate buffer, pH 7.2 (11650; Electron Microscopy Sciences, Hatfield, PA, USA), at room temperature for 1 h, then washed in cacodylate buffer for a further 30 min. The samples were postfixed in 1% osmium tetroxide (19150; Electron Microscopy Sciences, Hatfield, PA, USA) for 1 h at room temperature, then dehydrated through graded alcohol series (VWR Chemicals, 20821.296), and embedded in Epon 812 medium (45345; Sigma Aldrich, St. Louis, MO, USA). Ultrathin sections of 80 nm were cut using a Leica Ultracut UCT Ultramicrotome (Leica-Reichert; Leica Microsystems; Wetzlar, Germany), contrasted with uranyl acetate and examined at 120 kV with a JSM-4000 (JEOL; Tokyo, Japan) electron microscope. Images were captured digitally by an Orius 1000 (Gatan, Abingdon, UK) camera.

#### Statistical analysis

The count of lysosomes was performed in TEM grids containing the cross-sections of KGN cells loaded with apoptotic oocytes (24 cross-sections), POS (12 cross-sections) and unloaded control KGN cells (8 cross-sections). Graph Pad Prism Software (San Diego, CA, USA) was used to conduct statistical analysis using one-way ANOVA followed by Bonferroni posthoc test. Differences were considered statistically significant for a value of  $P < 0.05$  and  $P < 0.001$ .

## Ethical approval

Human samples were provided by GERMETHEQUE Biobank (BBMRI, France). All patients gave a specific written informed consent. The study was approved by local Ethics Committee (Advice 20-190-404).

## Results

### GCs ingest apoptotic oocytes and other apoptotic substrates

Our first challenge was to ensure that the GC ingest the apoptotic oocytes. Therefore, we incubated the primary culture of human GC with apoptotic oocytes, and then performed IF analysis. We used FITC-labeled oocytes to follow their path after the incubation with cultured primary GC. In parallel experiments we incubated the cells with the isolated fraction of rat POS.

Figure 1 a, a', b, and b' shows that primary cultures of human GC interacted with FITC-labeled apoptotic substrates, so that the green-colored points were found in association with the cells. Some green points were located at the cell periphery (the others exhibited peri-nuclear localization. Not only primary cultures of GC, but also human granulosa KGN cell line interacted with apoptotic substrates (apoptotic oocytes, POS or the fragments of apoptotic KGN cells obtained after the induction of apoptosis by ceramide) (Fig.1, c, d; Supplementary Fig. S1a). Figure 1 (c, d) shows green colored fragments of apoptotic substrates in close association with the cultured KGN cells in both the cell periphery and next to the nuclei. Because of the transparency of the plasma membrane, it is often problematic to discern by light microscopy the substrates bound to the plasma membrane and/or ingested by the cells (Yefimova et al., 2018). Therefore, to ensure that apoptotic oocytes and other apoptotic substrates were ingested by the GC, we then proceeded with TEM. TEM analysis allowed us to reveal the fragments of apoptotic oocytes, and other apoptotic substrates (the fragments of apoptotic KGN cells, the POS) in the



cytoplasm of cultured GC (Fig.1 e-g). In agreement with our IF data, the fragments of apoptotic substrates were found in the periphery of the GC, enclosed in phagocytic vacuoles (Fig.1 f, g), and more deeply in cell cytoplasm (Fig.1 f, g). Of note that in all cases the ingested apoptotic substrates were enclosed in single-membrane phagosome vacuole.

Thus, the cultured GC exhibited the ability to ingest the apoptotic oocytes and other apoptotic substrates. It was then of interest to obtain insights into the molecular mechanisms providing the ingestion and further management of ingested substrates by the GC.

#### Incubation of GCs with apoptotic substrates engages phosphorylation of MERTK

The primary response of the phagocyte involves the activation of specific receptors, which mediates reorganization of the actin cytoskeleton in order to form a phagocytic cup, and to ingest prey (Yefimova et al., 2018).

MERTK mediates the ingestion of apoptotic substrates in the testis and in the retina (Duncan et al., 2003; Yefimova, 2013). Because the isolated fraction of POS is a practical tool to study MERTK activation and LAP engagement in other phagocytic cells (Kim et al., 2013; Yefimova et al., 2013), we first incubated the KGN cells with POS in order to look for the distribution of phosphorylated MERTK. During the classical phagocytosis process, phagocytic cups harboring engulfed substrates co-localize with the activated phagocytosis receptors (Freeman & Grinstein, 2014). Confocal analysis showed that phospho-MERTK clusters did co-localize on the sites of contact of apoptotic substrate with the GC (Fig. 2 a, b). Co-localisation analysis revealed that  $58.8 \pm 4.1\%$  of substrate co-localized with  $54.98 \pm 4.5\%$  of clustered phosphorylated receptors (Fig. 2 c).

WB analysis confirmed the phosphorylation of MERTK during incubation of KGN cells with the isolated fraction of POS (Fig. 2 d). Remarkably, the incubation of KGN cells with apoptotic oocytes also resulted in MERTK phosphorylation, which gradually increased over time (Fig. 2 e), suggesting the involvement of MERTK in the primary phagocytosis response by KGN

cells. Incubation of KGN cells with apoptotic oocytes led to more pronounced phosphorylation of MERTK compared to that with ROS, as shown in the quantification data (Fig. 2 d, e).

MERTK signaling results in the recruitment of motor molecule myosin II, which facilitates substrate moving inside the phagocytes (Strick et al., 2009). In phagocytic cells from the retina and testis, this is heralded by the formation of myosin II clumps on the site of contact of phagocyte with prey. Therefore, we then studied the distribution of myosin II in KGN cells exposed to apoptotic substrates. Confocal analysis confirmed the clumping of myosin II on the sites of contact with apoptotic substrates (Fig. 2, f-h). Co-localization analysis showed that  $67.02 \pm 9.82\%$  of myosin II clumps co-localized with the fragments of apoptotic substrates (Fig. 2 i). Thus, the data obtained supported implication of the phagocytosis receptor MERTK in the primary phagocytosis response by the GC.

Uptake of apoptotic substrates but not of inert microspheres involves a fast lipidation of LC3 protein in GC

A major difference between LAP and classical phagocytosis is the accumulation of the lipidated form of LC3 protein (LC3-II). A major difference between LAP and conventional autophagy is a very short time taken for the accumulation of LC3-II. (Kim et al., 2013; Klionsky et al., 2016).

The uptake of synthetic inert microspheres does not engage LAP in phagocyte cells (Martinez et al., 2011), so that the phagosomes carrying the inert beads fail to contain LC3 and other LAP-related proteins (Martinez et al., 2011). Therefore, we then compared by IF the immunodistribution of LC3 protein in KGN cells fed with the inert fluorescent microspheres or with POS. Figure 3 a, b shows that anti-LC3 antibody stains the cytoplasm and intracellular vesicles in KGN cells. In cells exposed to POS, the green dots corresponding to LC3 protein co-localized with red anti-rhodopsin immunostaining (Fig. 3 a). On the contrary, these green dots

were not associated with fluorescent microspheres (Fig. 3 b). This suggests the involvement of LAP in the management of POS, but not of fluorescent beads.

Using WB we compared the expression of LC3 protein in the lysates of GC incubated with the inert microspheres and with the POS. Figure 3 c (upper panel, + beads) shows that in the lysates of KGN cells fed with the microspheres, the soluble form of LC3 protein (LC3-I, 17 kDa band) predominated on the blots at all times of incubation. In contrast, in the lysates from the GC incubated with POS (Figure 3 c, upper panel, + POS) a progressive increase of the lipidated form of LC3 protein (LC3-II, 14 kDa) was detected, starting from 30 min of incubation. Such early conversion of LC3-I to LC3-II during the uptake of POS (but not of microspheres) strongly suggests the involvement of LAP in the management of apoptotic substrates by GC. A kinetic study showed an increase of lipidated form of LC3 protein over time (Fig. 3c, bottom panel, left side) during the uptake of POS. The accumulation of LC3-II protein was also detected in GC fed with the fragments of apoptotic oocytes (Fig.3 c, bottom panel, right side). Of note is that the accumulation of LC3-II in cell lysates was associated with the progressive decrease of the intensity of GAPDH band used as housekeeping gene, probably due to the activation of degradation processes. Therefore, in our subsequent kinetic experiments we normalized WB data to time 0 (cells + phagocytosis substrate at the time 0).

Confocal microscopy followed by 3D reconstruction revealed LC3 protein on the surface of KGN cells in phagocytic cups containing POS (Fig. 3 d, e, f), and in the cytoplasm of KGN cells together with the ingested fragments of POS (Fig. 3 e, f). Quantitative co-localization analysis showed the partial co-localization of POS with LC3 protein (Fig. 3 g). Thus,  $10.6 \pm 3.0\%$  of phagocytosis substrates co-localized with  $43.1 \pm 9.7\%$  of LC3-stained structures (the ratio LC3/substrate = 4.07). Long-term kinetic experiments attested the gradual increase of the lipidation of LC3 protein over time (0-6h), supporting the continuity of the process (Fig. 3 h).

We used an antibody against the main protein of the zona pellucida, zona pellucida glycoprotein 3 (ZP3), to immunolocalize the fragments of apoptotic oocytes taken by the GC. As

in the previous case (i.e. incubation with POS), anti-LC3 antibody stained phagocytic cups, containing the fragments of apoptotic oocytes, and those ingested by the GC (Fig. 3, i-l). The rapid conversion of LC3-I to LC3-II (starting from 30 min of incubation; Fig. 3 c) and increase in LC3-II/LC3I ratio over time was also detected in the lysates from KGN cells exposed to the fragments of apoptotic oocytes (Fig. 3 m). Collectively these data support the involvement of LAP in the management of apoptotic substrates by the GC.

#### Uptake of apoptotic substrates by GC engages autophagy proteins

In contrast to classical phagocytosis cups, those formed during LAP contain several autophagy proteins (Kim et al., 2013; Panneerdoss et al., 2017; Duan et al., 2018). Thus, Beclin1 and ATG5 proteins are known to be recruited to phagosomal membranes as a very early event in LAP (Martinez et al., 2011; Kim et al., 2013; Li et al., 2013). Therefore, we then investigated the distribution of Beclin1 and ATG5 in human granulosa KGN cells exposed to apoptotic substrates, by confocal immunofluorescent microscopy. We also followed by WB the expression of these proteins in KGN cells during their incubation with apoptotic oocytes and/or with the POS.

Figure 4 shows the immunodistribution of ATG5 and Beclin1 proteins in KGN cells, exposed to POS (Fig. 4 a, b, j, k) and to apoptotic oocytes (Fig. 4 e-h, n-q). By confocal analysis we demonstrated that both ATG5 and Beclin1 proteins are present in the cytoplasm of KGN cells, and in association with intracellular vesicles. Confocal slicing and 3D analysis of GC exposed to POS and/or apoptotic oocytes revealed strong co-localisation of apoptotic substrates with autophagy proteins ATG5 and Beclin1 (Fig. 4 a, b, e-h, j, k, n-q). Indeed, ATG5 and Beclin1 co-localized with apoptotic substrates on the surface of KGN cells during the formation of phagocytic cups and after their ingestion in the cytoplasm of KGN cells. This corroborates the contribution of autophagy proteins to the formation and maturation of the phagosome/LAPosome

in KGN cells. As showed in control experiments, ATG5 and Beclin 1 proteins did not co-localize with the inert microspheres ingested by KGN cells (Supplementary Fig. S1 b, c).

Quantitative co-localization analysis revealed the partial co-localization of phagocytosis substrates with autophagy proteins. Thus,  $10.8 \pm 1.7\%$  of phagocytosis substrates co-localized with  $13.7 \pm 6.2\%$  of ATG5-stained vesicles (the ratio ATG5/substrate = 1.26); and  $15.9 \pm 2.7\%$  phagocytosis substrates co-localized with  $31.0 \pm 7.2\%$  Beclin1-stained vesicles (the ratio Beclin1/substrate = 1.95) (Fig. 4 c, l).

We also analyzed the lysates of KGN cells for the presence of ATG5 and Beclin1 proteins by WB at different times of incubation with apoptotic oocytes and POS. Both ATG5 and Beclin1 proteins were found in the lysates of KGN cells at all times of incubation (from 0h to 6h) (Fig. 4 d, i, m, r). Densitometry analysis of blots revealed a relative increase of ATG5 proteins during the incubation of KGN cells with the apoptotic oocytes (Fig. 4 i), while the expression of Beclin 1 protein did not vary during the same incubation period. We also explored the expression of ATG7 protein, which is specifically involved in LAP (Klionsky et al., 2016). WB analysis shows that KGN cells loaded with apoptotic substrates stably expressed ATG7 during the incubation period (Supplementary Fig. S1d). Thus, the uptake of apoptotic substrates by the GC engages autophagy proteins, as occurs after LAP activation.

#### Rapamycin treatment slows down the ingestion of apoptotic substrates by GC

Phagocytosis, autophagy and LAP utilize lysosomes for cargo degradation (Muniz-Feliciano et al., 2017). In rodent retinal pigment epithelium (RPE) cells under physiological condition, phagocytosis and autophagy processes reach their peak at different times of day. This avoids the competition for lysosomal resources *in vivo* (Muniz-Feliciano et al., 2017) and suggests a balance between autophagy and LAP in phagocytes. Indeed, starvation-induced autophagy impaired the degradation of POS (Kim et al., 2013; Muniz-Feliciano et al., 2017).

Therefore, it was of interest to explore whether the induction of autophagy in GC would influence the uptake of apoptotic substrates.

Because of the involvement of mTOR (mechanistic target of rapamycin [serine/threonine kinase])-dependent autophagy in follicular development (Choi et al., 2014), we chose rapamycin to induce autophagy in the GC. WB analysis of cell lysates confirmed the lipidation of LC3 protein in rapamycin-treated cells (Supplementary Fig. S1 e). Then, we incubated rapamycin-treated and untreated cells with POS and analyzed their distribution using a phagocytosis test, which discriminates between bound and ingested substrates (Yefimova et al., 2013; Yefimova et al., 2018). Figure 4 s (top panel) shows that in control cells the red staining corresponding to POS was mainly associated with small fragments, located in cell cytoplasm. The large fragments of POS, attached to plasma membrane, were less frequent. On the contrary, in rapamycin-treated cells these large fragments of POS predominated (Fig. 4 s, bottom panels). The large fragments of POS strongly colocalized with anti-LC3 immunoreactivity (green). In merged pictures from rapamycin-treated cells (Fig. 4 s, bottom panels) the fragments of POS appeared to be encircled with anti-LC3 immunostaining, suggesting their engulfment in phagocytic cups.

As shown in quantification analysis, both control and rapamycin-treated GC progressively accumulated the POS over time (Fig. 4 t). At all times of incubation, the total amount of POS (bound + ingested) associated with KGN cells was similar in rapamycin-treated and untreated specimens (Fig. 4 t). Nevertheless, the phagocytosis test revealed that the amount of ingested POS was dramatically reduced in rapamycin-treated GC compared to control cells. This effect was observed starting from 30 min of incubation and continued at all periods studied (up to 2 hours) (Fig. 4 t). The phagocytosis test supported the data from IF analysis, which attested the predominance of phagocytic cups, but not of intracellular fragments of POS, in rapamycin-treated cells (Fig. 4 s).

Degradation of apoptotic substrates by GC requires lysosomal proteolysis, but not the depletion of p62 protein

Examination of tissue sections shows that phagocytosis of apoptotic substrates by both Sertoli and RPE cells results in an increase in number of lysosomes (Chemes et al., 1986; LaVail, 1976). Therefore, it was then of interest to look at the content of lysosomes in the GC during the uptake of apoptotic oocytes and/or POS using different techniques.

We first used a classical Gomori method (Allison & Mallucci, 1969) for acid phosphatase activity to assess lysosomal enzymes cytochemically. Using the cytochemical technique in control GC, lysosomes were identified as brown vesicles of identical size located next to the nucleus (Fig. 5 a). In the absence of phagocytosis each granulosa cell contained on average  $9.3 \pm 0.3$  (n=110) Gomori-stained points, so that the ratio of brown-colored area per cell corresponded to a value of  $6.4 \cdot 10^{-4} \pm 0.6 \cdot 10^{-4}$  (n=110). Uptake of either apoptotic oocytes or POS resulted in a dramatic increase of Gomori staining in the GC (Fig. 5 b, c). In both cases, the brown points exhibited a variable size, shape and location in the GC. Some of Gomori-stained vesicles (Fig. 5 b, c) concentrated on the cell periphery, while others were detected next to the nucleus, or encircled plasma membrane. Quantification revealed a huge increase in Gomori staining in cells challenged with oocytes and POS (Fig. 5 d, upper panel), which corresponded to the values of  $1.1 \cdot 10^{-2} \pm 0.1 \cdot 10^{-2}$  (n=250) and  $1.4 \cdot 10^{-2} \pm 0.2 \cdot 10^{-2}$  (n=250), respectively.

Cathepsin D is the main lysosomal protease, involved in the degradation of different substrates by various phagocytes, including the Sertoli cells and the RPE cells (Zimmerman et al., 1983; Igdoura et al., 1995; Benes et al., 2008). Cathepsin D is also expressed in the GC. Moreover, its activity increases in the atretic follicles (Dhanasekaran, et al. 1983). Therefore, we then studied the immunodistribution of Cathepsin D in the KGN cells incubated with the POS and with the fragments of apoptotic oocytes.

In KGN cells exposed to the fragments of POS, the anti-Cathepsin D immunostaining presented a vesicular pattern, implying association of the protein with the lysosomes (Fig. 5, e-

h). Quantification demonstrated that the amount of Cathepsin D-stained vesicles increased over time during the incubation of KGN cells with the POS (Fig. 5 d, lower panel). In KGN cells exposed to apoptotic oocytes, anti-Cathepsin D immunostaining strongly concentrated around the fragments of apoptotic oocytes undergoing the process of the ingestion or which were already ingested by the cell (Fig. 5 i-k). The 3D reconstruction (Fig. 5 k) shows that anti-Cathepsin D immunostaining formed the “coats” encircling the fragments of apoptotic oocytes, which were located on the cell surface and in the cytoplasm (Fig. 5 i-k, lower panels, selections 1-4).

We examined by WB the content of Cathepsin D in the lysates of KGN cells fed with POS and/or apoptotic oocytes. Cathepsin D is produced in the inactive form, pre-proCathepsin D, which is quickly converted into proCathepsin D (Lai et al., 2000) and then to biologically active Cathepsin D. As usual, both proCathepsin D 56 (kDa) and Cathepsin D are present on the blots from cell lysates in differential proportional relationships (Lai et al., 2000). In our hands, the Cathepsin D from cell lysates of KGN cells migrated as a single band of 34 kDa. We did not detect on the blots an inactive 56 kDa form, probably because of the fast conversion of newly synthesized proCathepsin D in its active form (Fig. 5 l). Of note, is that the proCathepsin D (56 kDa) was clearly detected in cell lysates from the human RPE cell line (hTERT-RPE1) incubated with the POS, used as a control (Supplementary Fig. S1 f). In agreement with our quantification study, WB analysis also demonstrated the increase of Cathepsin D content during the incubation of KGN cells with the POS, and with the apoptotic oocytes (Fig. 5 i).

Thus, cytochemical, immunocytochemical, and WB experiments revealed an increase of lysosome-related parameters during phagocytosis by GC. Then, TEM examination of ultrathin sections from KGN cells challenged with apoptotic substrates was undertaken. Figure 5 shows that lysosome content (both primary and secondary lysosomes) dramatically increases during the exposure of KGN cell cultures to apoptotic oocytes and POS (Fig. 5 m, n, o). Quantification revealed a 4-fold increase in lysosome content after 12h of phagocytosis of apoptotic substrates



by the GC, compared to control (absence of phagocytic substrate) (Fig. 5, p). This is in good agreement with previous results, attesting the contribution of lysosomes to the management of ingested apoptotic substrates.

p62 protein is a specific adaptor involved in autophagy. It selectively recognizes autophagic cargo and mediates its engulfment into autophagosomes (Lippai & Löw, 2014). When lysosome-dependent autophagy degradation is activated the content of p62 decreases, whereas the LAP-dependent degradation does not modify the levels of p62 in the cells (Muniz-Feliciano et al., 2017). Therefore, we then studied by WB the content of p62 protein in KGN cells challenged with POS and/or apoptotic oocytes. WB analysis did not reveal any variation in the content of p62 protein in KGN cells at all times of incubation with POS (Fig. 5 q) or apoptotic oocytes (Fig. 5 r), thereby supporting the involvement of LAP in their degradation.

Collectively, we concluded that GC efficiently ingest and degrade apoptotic oocytes and other apoptotic substrates in a process strongly resembling LAP.

## Discussion

The removal of apoptotic cells and cell debris that are continuously produced during the lifespan of a tissue is a vital task in all tissues of the body (Arandjelovic & Ravichandran, 2015). This task is routinely achieved by professional phagocytes, which are the cells of hematopoietic origin such as macrophages, dendritic cells and microglia. Professional phagocytes ingest and destroy apoptotic substrates in almost all tissues of the body, except the retina and the testis. The retina and the testis, which are isolated from the blood, were classically considered as exceptions to the general rule because the removal of apoptotic substrates was achieved by resident epithelial cells (Nakanishi et al., 2011; Penberthy et al., 2018). Here we demonstrate that the ovary is a third example of a tissue that uses the same principle as retina and the testis to remove apoptotic substrates through the functioning of local epithelial cells.

We show here for the first time that human GC maintained *in vitro* (primary culture and KGN cell line) efficiently ingest and destroy apoptotic oocytes. To this end, we show that GC use, in part, the LAP mechanism - a hybrid process in which a classical phagocytosis is supported by autophagy degradation machinery. Being triggered by the uptake of extracellular cargoes, but not by autophagy inducers, LAP is a separate process, which differs from phagocytosis and autophagy in their morphological, molecular and temporal aspects. Therefore, in this work we used different approaches, such as ultrastructure examination, and kinetic and molecular studies, to identify the involvement of LAP in the management of apoptotic substrates. All of these approaches supported the involvement of LAP, but not of autophagy, in the processing of apoptotic substrates by GC.

LAP is a tightly regulated mechanism in which the efficacy of substrate clearance determines the rate of the ingestion of apoptotic substrates owing to a regulatory feedback loop (Teplova et al., 2013). In the blood-separated retina and testis, ingestion of apoptotic substrates largely relies upon activation of the phagocytosis receptor MERTK, a member of the TAM (Tyro3, Axl, MERTK) family of tyrosine kinases involved in various aspects of cell life (Lemke & Rothlin, 2008). Being expressed by retinal pigmented epithelial cells and by the somatic Sertoli cells in testis, TAM receptors play a pivotal role for vision and male reproduction function (Duncan et al., 2003; Lemke & Rothlin, 2008). Genetic ablation or mutation of *MERTK* results in irreversible blindness in human and animal models (Duncan et al., 2003). When combined with the mutations in *Tyro3* and *Axl*, triple mutant TAM<sup>-/-</sup> mice exhibit abnormal spermatogenesis, infertility in males and reduced fertility in females (Lu et al., 1999): the latter observation strongly indicates the importance of TAM receptors in the molecular mechanisms sustaining female fertility. Remarkably, transcriptomic analysis of bovine GC from small antral follicles undergoing atresia revealed a 4-fold increase of MERTK expression (Hatzirodos et al., 2014), supporting the idea of the role of GC in removing apoptotic oocytes.

A dysfunction in both the MERTK receptor and LAP mechanism contributes to establishment of the lupus-like autoimmune status associated with sustained inflammation (Scott et al., 2001; Lemke & Rothlin, 2008; Rothlin, et al., 2015; Martinez et al., 2016). Indeed, in normal situations, LAP is a rapid “immunologically silent” process in which the apoptotic substrates are managed at the early stages of apoptosis. However, once the integrity of the plasma membrane is lost due to the secondary necrosis of late-stage apoptotic cells, the released cellular contents can engage receptors for damage-associated molecular patterns and contribute to immune responses to self antigens (Janko et al., 2011; Arandjelovic & Ravichandran, 2015). Remarkably, the human ovary is commonly the target of an autoimmune attack leading to ovarian dysfunction, manifested as premature ovarian failure (POF), polycystic ovary syndrome (PCOS), unexplained infertility, or endometriosis (Komorowska, 2016). In the case of POF, the autoantibodies to ovarian antigens have been clearly documented in numerous studies (Nelson, 2009; Gleicher et al., 2015). Besides, inflammation plays a considerable role in the mechanism of POF, and controlling the development of inflammatory status may be one of the methods to treat POF (Huang et al., 2019).

One of the major functions ascribed to LAP is to promote phagosome maturation through the recruitment of autophagy proteins (Martinez et al., 2011). However, recent reports suggest that this requirement is not universal. Thus, in mouse embryonic fibroblasts and in bone marrow-derived macrophages, maturation of the phagosome was not affected after ablation of the *ATG5* and *ATG7* genes (Cemma et al., 2016), highlighting the complexity and cell-specificity of LAP in different phagocytosis models. In our KGN cell model, we observed an increase of the expression of ATG5 protein during phagocytosis of apoptotic oocytes, while those of ATG7 did not vary. The formation of phagocytic cups and the ingestion of apoptotic substrates progress through activation of a downstream effector, Ras-related C3 botulinum toxin substrate (RAC1), which mediates actin reorganization (Kim et al., 2013; Teplova et al., 2013; Panneerdoss et al., 2017; Duan et al., 2018). While the order of events in the signaling pathways remains an

unaddressed question (Heckmann et al., 2017), the recruitment of autophagy proteins seems to be necessary to sustain MERTK-mediated ingestion. Indeed, the invalidation of *Atg7* and *Beclin1* genes results in the decreased expression of phagocytosis receptor MERTK and integrin beta5, which co-operate with MERTK to facilitate the ingestion (Teplova et al., 2013). Noteworthy, along with the increase of MERTK (Hatzirodos et al., 2014) GC from the atretic follicles increase the expression of autophagy proteins (Choi et al., 2010), suggesting the co-operation of both partners during the process of atresia. In agreement with these *in vivo* observations are the results from our *in vitro* model, in which the phosphorylation of MERTK and lipidation of LC3 protein progressed over time to provide the ingestion of apoptotic substrates. In fact, the early time-course of LC3 lipidation (starting from 30 min of incubation with apoptotic substrates) is more compatible with the activation of LAP than autophagy in GC.

Our data show that the exposure of GC to apoptotic oocytes and/or POS induced a significant increase in lysosome number. Of note is that a strong increase of lysosome quantity also occurs in the Sertoli cells from seminiferous tubules and in RPE cells following phagocytosis of spermatid residual bodies and of POS (Chemes et al., 1986; LaVail, 1976). On the contrary, the activation of autophagy has also been shown to dramatically reduce the number of lysosomes in cells (Xu & Ren, 2015). In line with this, the response of GC fits with a classical response of phagocyte cells, which boost lysosome gene expression and lysosome number to handle successive rounds of phagocytosis (Gray et al., 2016; Wong et al., 2017).

Cathepsin D, a key lysosomal protease (Benes et al., 2008), which ensures the degradation of apoptotic substrates in the retina and the testis (Bosch et al., 1993; Saewu et al., 2012), is expressed in GC (Dhanasekaran & Moudgal, 1986). Remarkably, the expression of Cathepsin D increases in GC from early atretic follicles (Dhanasekaran & Moudgal, 1983; Dhanasekaran & Moudgal, 1989). We also detected by WB experiments a progressive increase of Cathepsin D protein in GC exposed to either POS or apoptotic oocytes. One interesting finding was the absence of a protein band corresponding to inactive proCathepsin D 56 (kDa) on

the blots from the lysates of GC challenged with phagocytosis substrates, although this band was clearly seen on the blots from the lysates of hTERT-RPE1 cells used as control. This could either indicate some peculiarities in the processing of Cathepsin D, or the rapid conversion of the enzyme from the inactive to active state by GC.

Autophagy and LAP are distinct pathways that use many of the same mediators and must compete for cellular resources (Muniz-Feliciano et al., 2017). In agreement with this, in our study we show that the induction of autophagy in GC negatively influences the processing of nascent phagosomes (Lu & Zhou, 2012), as reported for RPE cells (Kim et al., 2013; Muniz-Feliciano et al., 2017). Another reliable criterion to support the involvement of LAP in lysosomal degradation is the level of p62 protein. p62 is a special adaptor for autophagy degradation (Klionsky et al., 2016), therefore the level of p62 decreases when autophagy is activated but remains unchanged during LAP (Muniz-Feliciano et al., 2017). In line with this, our study supports the idea of the involvement of LAP, but not of autophagy, in the degradation of apoptotic substrates ingested by the GC.

To date, the information on regulation of LAP is scarce. A study on retinal pigmented epithelial cells demonstrated that autophagy-inducing factors suppress LAP (Muniz-Feliciano et al., 2017). One of these factors is the epidermal growth factor receptor (EGFR), whose activation promotes autophagy and suppresses LAP. EGFR is expressed in GC (Shimada & Yamashita, 2011). Furthermore, its activation is induced by FSH, which is a key regulator of folliculogenesis and spermatogenesis (Jégou, 1993; Shimada & Yamashita, 2011). Exogenous FSH is widely used to prevent GC apoptosis and follicular atresia. Moreover, administration of FSH induces autophagy in GC, promoting follicular growth and development (Zhou et al., 2017), but not atresia. On the other hand, a study of the seminiferous tubules demonstrated an inhibitory effect of FSH on the ingestion of apoptotic substrates by the Sertoli cells (Pineau et al., 1991). Overall, these data give some indirect indications of the possible role of FSH in the regulation of LAP-

dependent removal of apoptotic oocytes by the GC, opening a new view on the treatment of POF and PCOS.

In summary, here we demonstrate for the first time that blood-barrier forming epithelial GC can act as powerful non-professional phagocytes in maintaining ovarian homeostasis. This is achieved through the removal from ovarian tissue of apoptotic substrates by means of unconventional autophagy-assisted phagocytosis. Cleaning of apoptotic oocytes by the surrounding GC seems likely to be a physiological mechanism involved in follicular atresia. A better understanding of this physiological process could open new strategies in the treatment of ovarian dysfunctions associated with the imbalanced content of germ cells in the ovaries, such as POF and/or PCOS.

### **Acknowledgments**

We thank Dr. A Cantereau-Becq for confocal imaging, Mr. A Dupont and Mr. G Gukasyan for excellent technical assistance. We thank Prof. V Catros and Dr. JC Hervé for critical reading of the manuscript. We thank H2P2 platform and MRIC platform from Rennes University, and Image UP platform from Poitiers University. MGY was welcomed as invited Professor by CHU de Rennes. MGY acknowledges Direction de la Recherche Clinique du CHU de Rennes.

### **Authors' roles**

MGY carried out study design, execution, analysis of data, and writing/revising the manuscript. CL and ACM participated in human granulosa cell collection and immunocytochemistry experiments. ABurel and MTL participated in electron microscopy experiments. ABashamboo and CE participated in primary culture setting up. CP, SV, ASN and SJ recruited IVF samples. BJ participated in the structuration of the team research funding and

manuscript revision. NB was involved in study conception, data analysis, and manuscript revision. CR is the senior author involved in study conception, data analysis, and manuscript revision. All authors read and approved the final manuscript.

**Funding**

The study was funded by Rennes Metropole (AIS 2015) and Agence de BioMédecine. This work was supported by funding from Université de Rennes1, Institut National de la Santé et de la Recherche Médicale (INSERM) and CHU de Rennes. A. Bashamboo is funded in part by the program Actions Concertées Interpasteuriennes (ACIP) and a research grant from the European Society of Pediatric Endocrinology. This work is supported by the Agence Nationale de la Recherche Grants ANR-17-CE14-0038 and ANR-10-LABX-73.

**Conflict of interest**

None declared.

**References**

- Allison AC, Mallucci I. Histochemical studies of lysosomes and lysosomal enzymes in virus-infected cell cultures. *J Exp Med* 1965;**121**:463-476.
- Amer AO, Swanson MS. Autophagy is an immediate macrophage response to Legionella pneumophila. *Cell Microbiol* 2005;**7**:765-78.
- Arandjelovic S, Ravichandran KS. Phagocytosis of apoptotic cells in homeostasis. *Nat Immunol* 2015;**16**:907-917.

- 761 Bandyopadhyay U, Overholtzer M. LAP: the protector against autoimmunity. *Cell Res*  
762 2016;**26**:865–866.
- 763 Benes P, Vetvicka V, Fusek M. Cathepsin D-many functions of one aspartic protease. *Crit*  
764 *Rev Oncol Hematol* 2008;**68**:12-28.
- 765 Bosch E, Horwitz J, Bok D. Phagocytosis of outer segments by retinal pigment epithelium:  
766 phagosome-lysosome interaction. *J Histochem Cytochem* 1993;**41**:253-263.
- 767 Cemma M, Grinstein S, Brumell JH. Autophagy proteins are not universally required for  
768 phagosome maturation. *Autophagy* 2016;**12**:1440–1446.
- 769 Chemes H. The phagocytic function of Sertoli cells: a morphological, biochemical, and  
770 endocrinological study of lysosomes and acid phosphatase localization in the rat testis.  
771 *Endocrinology* 1986;**119**:1673-1681.
- 772 Choi J, Jo M, Lee E, Choi D. AKT is involved in granulosa cell autophagy regulation via  
773 mTOR signaling during rat follicular development and atresia. *Reproduction* 2013;**147**:73–  
774 80.
- 775 Choi JY, Jo MW, Lee EY, Yoon BK, Choi DS. The role of autophagy in follicular  
776 development and atresia in rat granulosa cells. *Fertil Steril* 2010;**93**:2532-2537.
- 777 Davis MA, Flaws JA, Young M, Collins K, Colburn NH. Effect of ceramide on intracellular  
778 glutathione determines apoptotic or necrotic cell death of JB6 tumor cells. *Toxicol Sci*  
779 2000;**53**:48-55.
- 780 Dhanasekaran N, Moudgal NR. Studies on follicular atresia: role of tropic hormone and  
781 steroids in regulating cathepsin-D activity of preantral follicles of the immature rat. *Mol Cell*  
782 *Endocrinol* 1986;**63**:133-142.



- 783 Dhanasekaran N, Moudgal NR. Studies on follicular atresia: role of gonadotropins and  
784 gonadal steroids in regulating cathepsin-D activity of preovulatory follicles in the rat. *Mol*  
785 *Cell Endocrinol* 1989;**63**:133–142.
- 786 Dhanasekaran N, Sheela Rani CS, Moudgal NR. Studies on follicular atresia: lysosomal  
787 enzyme activity and gonadotropin receptors of granulosa cells following administration or  
788 withdrawal of gonadotropins in the rat. *Mol Cell Endocrinol* 1983;**33**:97-112.
- 789 Duan Z, Chen Q, Du L, Tong J, Xu S, Zeng R, Ma Y, Chen X, Li M. Phagocytosis of  
790 *Candida albicans* Inhibits Autophagic Flux in Macrophages. *Oxid Med Cell Longev*  
791 2018;**2018**:4938649
- 792 Duncan JL, LaVail MM, Yasumura D, Matthes MT, Yang H, Trautmann N, Chappelov AV,  
793 Feng W, Earp HS, Matsushima GK, Vollrath D. An RCS-like retinal dystrophy phenotype in  
794 mer knockout mice. *Invest Ophthalmol Vis Sci* 2003;**44**:826-838.
- 795 Elmore S. Apoptosis: a review of programmed cell death. *Toxicol Pathol* 2007;**35**:495-516.
- 796 Finnemann SC, Bonilha VL, Marmorstein AD, Rodriguez-Boulan E. Phagocytosis of rod  
797 outer segments by retinal pigment epithelial cells requires alpha(v)beta5 integrin for binding  
798 but not for internalization. *Proc Natl Acad Sci U S A* 1997;**94**:12932-12937.
- 799 Freeman SA, Grinstein S. Phagocytosis: receptors, signal integration, and the cytoskeleton.  
800 *Immunol Rev* 2014;**262**:193-215.
- 801 Gaytán F, Morales C, Bellido C, Aguilar E, Sánchez-Criado JE. Ovarian follicle  
802 macrophages: is follicular atresia in the immature rat a macrophage-mediated event? *Biol*  
803 *Reprod* 1998;**58**:52-59.

- 804 Gleicher N, Kushnir VA, Barad DH. Prospectively assessing risk for premature ovarian  
805 senescence in young females: a new paradigm. *Reprod Biol Endocrinol* 2015;**13**:34.
- 806 Gray MA, Choy CH, Dayam RM, Ospina-Escobar E, Somerville A, Xiao X, Ferguson SM,  
807 Botelho RJ. Phagocytosis Enhances Lysosomal and Bactericidal Properties by Activating the  
808 Transcription Factor TFEB. *Curr Biol* 2016;**26**:1955-1964.
- 809 Hatzirodos N, Hummitzsch K, Irving-Rodgers HF, Harland ML, Morris SE, Rodgers RJ.  
810 Transcriptome profiling of granulosa cells from bovine ovarian follicles during atresia. *BMC*  
811 *Genomics* 2014;**15**:40.
- 812 Heckmann BL, Boada-Romero E, Cunha LD, Magne J, Green DR. LC3-Associated  
813 Phagocytosis and Inflammation. *J Mol Biol* 2017;**429**:3561-3576.
- 814 Huang Y, Hu C, Ye H, Luo R, Fu X, Li X, Huang J, Chen W, Zheng Y. Inflamm-Aging: A  
815 New Mechanism Affecting Premature Ovarian Insufficiency. *J Immunol Res*  
816 2019;**2019**:8069898.
- 817 Igdoura SA, Morales CR, Hermo L. Differential expression of cathepsins B and D in testis  
818 and epididymis of adult rats. *J Histochem Cytochem* 1995;**43**:545-557.
- 819 Itoh M, Yano A, Li X, Miyamoto K, Takeuchi Y. Limited uptake of foreign materials by  
820 resident macrophages in murine ovarian tissues. *J Reprod Immunol* 1999;**43**:55-66.
- 821 Janko C, Franz S, Munoz LE, Siebig S, Winkler S, Schett G, Lauber K, Sherif A, van der  
822 Vlag J, Herrmann M. CRP/anti-CRP antibodies assembly on the surfaces of cell remnants  
823 switches their phagocytic clearance toward inflammation. *Front Immunol* 2011;**2**:70.
- 824 Jégou B. The Sertoli-germ cell communication network in mammals. *Int Rev Cytol*  
825 1993;**147**:25-96.

- 826 Johnston RB Jr, Klemperer MR, Alper CA, Rosen FS. The enhancement of bacterial  
827 phagocytosis by serum. The role of complement components and two cofactors. *J Exp Med*  
828 1969;**129**:1275-1290.
- 829 Jungheim ES, Meyer MF, Broughton DE. Best practices for controlled ovarian stimulation in  
830 in vitro fertilization. *Semin Reprod Med* 2015;**33**:77-82.
- 831 Kasuya K. Elimination of apoptotic granulosa cells by intact granulosa cells and  
832 macrophages in atretic mature follicles of the guinea pig ovary. *Arch Histol Cytol*  
833 1997;**60**:175-184.
- 834 Katabushi H, Fukumatsu Y, Araki M, Suenaga Y, Ohtake H, Okamura H. Role of  
835 macrophages in ovarian follicular development. *Horm Res* 1996;**46** Suppl 1:45-51.
- 836 Kerr JFR, Wyllie AH, Currie AR. Apoptosis: a basic biological phenomenon with wide-  
837 ranging implications in tissue kinetics. *Br J Cancer* 1972;**26**:239–257.
- 838 Kim JY, Zhao H, Martinez J, Doggett TA, Kolesnikov AV, Tang PH, Ablonczy Z, Chan CC,  
839 Zhou Z, Green DR, Ferguson TA. Noncanonical autophagy promotes the visual cycle. *Cell*  
840 2013;**154**:365-376.
- 841 Klionsky DJ, Abdelmohsen K, Abe A, Abedin MJ, Abeliovich H, Acevedo Arozena A, et al.  
842 Guidelines for the use and interpretation of assays for monitoring autophagy (3rd edition).  
843 *Autophagy* 2016;**12**:1-222.
- 844 Komorowska B. Autoimmune premature ovarian failure. *Menopause Rev* 2016;**15**:210-214.
- 845 Lai CM, Robertson T, Papadimitriou J, Shen WY, Daw N, Constable IJ, Rakoczy  
846 PE. Controlled production of active cathepsin D in retinal pigment epithelial cells following  
847 adenovirus-mediated gene delivery. *Mol Ther* 2000;**2**:476-484.

- 848 LaVail MM. Rod outer segment disk shedding in rat retina: relationship to cyclic lighting.  
849 *Science* 1976;**194**:1071–1074.
- 850 Lemke G, Rothlin CV. Immunobiology of the TAM receptors. *Nat Rev Immunol*  
851 2008;**8**:327–336.
- 852 Li X, Prescott M, Adler B, Boyce JD, Devenish RJ. Beclin 1 is required for starvation-  
853 enhanced, but not rapamycin-enhanced, LC3-associated phagocytosis of *Burkholderia*  
854 *pseudomallei* in RAW 264.7 cells. *Infect Immun* 2013;**81**:271–277.
- 855 Lippai M, Löw P. The role of the selective adaptor p62 and ubiquitin-like proteins in  
856 autophagy. *Biomed Res Int* 2014;**2014**:832704.
- 857 Lu N, Zhou Z. Membrane trafficking and phagosome maturation during the clearance of  
858 apoptotic cells. *Int Rev Cell Mol Biol* 2012;**293**:269–309.
- 859 Lu Q, Gore M, Zhang Q, Camenisch T, Boast S, Casagrande F, Lai C, Skinner MK, Klein R,  
860 Matsushima GK, et al. Tyro-3 family receptors are essential regulators of mammalian  
861 spermatogenesis. *Nature* 1999;**398**:723–728.
- 862 Martinez J, Almendinger J, Oberst A, Ness R, Dillon CP, Fitzgerald P, Hengartner MO,  
863 Green DR. Microtubule-associated protein 1 light chain 3 alpha (LC3)-associated  
864 phagocytosis is required for the efficient clearance of dead cells. *Proc Natl Acad Sci U S A*  
865 2011;**108**:17396–17401.
- 866 Martinez J, Cunha LD, Park S, Yang M, Lu Q, Orchard R, et al. Noncanonical autophagy  
867 inhibits the autoinflammatory, lupus-like response to dying cells. *Nature* 2016;**533**:115–119.
- 868 Martinez J, Malireddi RK, Lu Q, Cunha LD, Pelletier S, Gingras S, Orchard R, Guan JL, Tan  
869 H, Peng J, Kanneganti TD, Virgin HW, Green DR. Molecular characterization of LC3-

- 870 associated phagocytosis reveals distinct roles for Rubicon, NOX2 and autophagy proteins.  
871 *Nat Cell Biol* 2015;**17**:893-906.
- 872 Masud S, Prajsnar TK, Torraca V, Lamers GEM, Benning M, Van Der Vaart M, Meijer AH.  
873 Macrophages target Salmonella by LC3-associated phagocytosis in a systemic infection  
874 model. *Autophagy* 2019;**15**:796-812.
- 875 Matsuda F, Inoue N, Manabe N, Ohkura S. Follicular growth and atresia in mammalian  
876 ovaries: regulation by survival and death of granulosa cells. *J Reprod Dev* 2012;**58**:44-50.
- 877 Mizushima N, Levine B, Cuervo AM, Klionsky DJ. Autophagy fights disease through  
878 cellular self-digestion. *Nature* 2008;**451**:1069-1075.
- 879 Mizushima N, Yoshimori T, Ohsumi Y. The role of Atg proteins in autophagosome  
880 formation. *Ann Rev Cell Dev Biol* 2011;**27**:107-132.
- 881 Mork L, Maatouk DM, McMahon JA, Guo JJ, Zhang P, McMahon AP, Capel B. Temporal  
882 differences in granulosa cell specification in the ovary reflect distinct follicle fates in mice.  
883 *Biol Reprod* 2012;**86**:37.
- 884 Muniz-Feliciano L, Doggett TA, Zhou Z, Ferguson TA. RUBCN/rubicon and EGFR regulate  
885 lysosomal degradative processes in the retinal pigment epithelium (RPE) of the eye.  
886 *Autophagy* 2017;**13**:2072-2085.
- 887 Nakanishi Y, Nagaosa K, Shiratsuchi A. Phagocytic removal of cells that have become  
888 unwanted: implications for animal development and tissue homeostasis. *Dev Growth Differ*  
889 2011;**53**:149-160.
- 890 Nelson LM. Clinical practice. Primary ovarian insufficiency. *N Engl J Med* 2009;**360**:606-  
891 614.

- 892 Ono Y, Nagai M, Yoshino O, Koga K, Nawaz A, Hatta H, Nishizono H, Izumi G,  
893 Nakashima A, Imura J, Tobe K, Fujii T, Osuga Y, Saito S. CD11c<sup>+</sup> M1-like macrophages  
894 (MΦs) but not CD206<sup>+</sup> M2-like MΦ are involved in folliculogenesis in mice ovary. *Sci Rep*  
895 2018;**8**:8171.
- 896 Panneerdoss S, Viswanadhapalli S, Abdelfattah N, Onyeagucha BC, Timilsina S,  
897 Mohammad TA, Chen Y, Drake M, Vuori K, Kumar TR, Rao MK. Cross-talk between miR-  
898 471-5p and autophagy component proteins regulates LC3-associated phagocytosis (LAP) of  
899 apoptotic germ cells. *Nat Commun* 2017;**8**:598.
- 900 Penberthy KK, Lysiak JJ, Ravichandran KS. Rethinking Phagocytes: Clues from the Retina  
901 and Testes. *Trends Cell Biol* 2018;**28**:317-327.
- 902 Pineau C, Le Magueresse B, Courtens JL, Jégou B. Study in vitro of the phagocytic function  
903 of Sertoli cells in the rat. *Cell Tissue Res* 1991;**264**:589-598.
- 904 Rothlin CV, Carrera-Silva EA, Bosurgi L, Ghosh S. TAM receptor signaling in immune  
905 homeostasis. *Annu Rev Immunol* 2015;**33**:355-391.
- 906 Saewu A, Asuvapongpatana S, Chotwiwatthanakun C, Tantiwongse A, Weerachatanukul  
907 W, Thitilertdech S. CathepsinD in human reproductive tissues: cellular localization in testis  
908 and epididymis and surface distribution in different sperm conditions. *J Androl* 2012;**33**:726-  
909 734.
- 910 Sanjuan MA, Dillon CP, Tait SW, Moshiah S, Dorsey F, Connell S, Komatsu M, Tanaka K,  
911 Cleveland JL, Withoff S, Green DR. Toll-like receptor signalling in macrophages links the  
912 autophagy pathway to phagocytosis. *Nature* 2007;**450**:1253-1257.

- 913 Scott RS, McMahon EJ, Pop SM, Reap EA, Caricchio R, Cohen PL, Earp HS, Matsushima  
914 GK. Phagocytosis and clearance of apoptotic cells is mediated by MER. *Nature*  
915 2001;**411**:207-211.
- 916 Shaha C, Tripathi R, Mishra DP. Male germ cell apoptosis: regulation and biology. *Philos*  
917 *Trans R Soc Lond B Biol Sci* 2010;**365**:1501-1515.
- 918 Shimada M, Yamashita Y. The key signaling cascades in granulosa cells during follicular  
919 development and ovulation process. *J Mamm Ova Res* 2011;**28**:25–31.
- 920 Siu MK, Cheng CY. The blood-follicle barrier (BFB) in disease and in ovarian function. *Adv*  
921 *Exp Med Biol* 2012;**763**:186-192.
- 922 Strick DJ, Feng W, Vollrath D. MERTK drives myosin II redistribution during retinal  
923 pigment epithelial phagocytosis. *Invest Ophthalmol Vis Sci* 2009;**50**:2427-2435.
- 924 Teplova I, Lozy F, Price S, Singh S, Barnard N, Cardiff RD, Birge RB, Karantza V. ATG  
925 proteins mediate efferocytosis and suppress inflammation in mammary involution.  
926 *Autophagy* 2013;**9**:459-475.
- 927 Wirawan E, Lippens S, Vanden Berghe T, Romagnoli A, Fimia GM, Piacentini M,  
928 Vandenabeele P. Beclin1: a role in membrane dynamics and beyond. *Autophagy* 2012;**8**:6-  
929 17.
- 930 Wong CO, Gregory S, Hu H, Chao Y, Sepúlveda VE, He Y, Li-Kroeger D, Goldman WE,  
931 Bellen HJ, Venkatachalam K. Lysosomal Degradation Is Required for Sustained  
932 Phagocytosis of Bacteria by Macrophages. *Cell Host Microbe* 2017;**21**:719-730.
- 933 Wu R, Van der Hoek KH, Ryan NK, Norman RJ, Robker RL. Macrophage contributions to  
934 ovarian function. *Hum Reprod Update* 2004;**10**:119-133.

- 935 Wu Y, Tibrewal N, Birge RB. Phosphatidylserine recognition by phagocytes: a view to a kill.  
936 *Trends Cell Biol* 2006;**16**:189-197.
- 937 Xu H, Ren D. Lysosomal physiology. *Annu Rev Physiol* 2015;**77**:57–80.
- 938 Yadav PK, Tiwari M, Gupta A, Sharma A, Prasad S, Pandey AN, Chaube SK. Germ cell  
939 depletion from mammalian ovary: possible involvement of apoptosis and autophagy. *J*  
940 *Biomed Sci* 2018;**25**:36.
- 941 Yefimova MG, Messaddeq N, Harnois T, Meunier AC, Clarhaut J, Noblanc A, Weickert JL,  
942 Cantereau A, Philippe M, Bourmeyster N, Benzakour O. A chimerical phagocytosis model  
943 reveals the recruitment by Sertoli cells of autophagy for the degradation of ingested  
944 illegitimate substrates. *Autophagy* 2013;**9**:653-666.
- 945 Yefimova MG, Messaddeq N, Meunier AC, Cantereau A, Jégou B, Bourmeyster N.  
946 Phagocytosis by Sertoli Cells: Analysis of Main Phagocytosis Steps by Confocal and  
947 Electron Microscopy. *Methods Mol Biol* 2018;**1748**:85-101.
- 948 Yefimova MG, Sow A, Fontaine I, Guilleminot V, Martinat N, Crepieux P, Canepa S,  
949 Maurel MC, Fouchécourt S, Reiter E, Benzakour O, Guillou F. Dimeric transferrin inhibits  
950 phagocytosis of residual bodies by testicular rat Sertoli cells. *Biol Reprod* 2008;**78**:697-704.
- 951 Yin Z, Pascual C, Klionsky DJ. Autophagy: machinery and regulation. *Microb Cell*  
952 2016;**3**:588-596.
- 953 Zhou J, Yao W, Li C, Wu W, Li Q, Liu H. Administration of follicle-stimulating hormone  
954 induces autophagy via upregulation of HIF-1 $\alpha$  in mouse granulosa cells. *Cell Death Dis*  
955 2017;**8**:e3001.



Zimmerman WF, Godchaux W 3rd, Belkin M. The relative proportions of lysosomal enzyme activities in bovine retinal pigment epithelium. *Exp Eye Res* 1983;**36**:151-158.

## Figure legends

**Figure 1** Human granulosa cells ingest the apoptotic substrates.

(a-d) Immunofluorescence (IF) pictures of the primary cultures of human granulosa cells (GC) (a, a', b, b') and human granulosa KGN cell line (c, d) incubated with apoptotic oocytes labeled with fluorescein isothiocyanate (FITC) (a, a', c), FITC-labeled photoreceptor outer segments (POS) (b, b') and FITC-labeled fragments of apoptotic KGN cells (d). Note the green-labeled fragments in cell periphery (arrow) and close to the nucleus stained with 4', 6 diamidino-2-phenylindol (DAPI) (arrowhead). a' and b' are the merged images of a and b with DIC projection. (e, f, g) Electron micrographs of human granulosa KGN cell line incubated with POS (e) with apoptotic oocytes (f), and with the fragments of apoptotic KGN (g) cells. Note the presence of apoptotic substrates inside the cells close to the plasma membrane (arrow) and more deeply next to the nucleus (n) (arrowhead).

**Figure 2** Primary phagocytosis response of human GC engages phosphorylation of c-mer proto-oncogene tyrosine kinase and myosin II clumping.

Confocal pictures of the human granulosa KGN cells (a, b, f-h) challenged with POS. (a, b) immunostaining with anti-phospho c-mer proto-oncogene tyrosine kinase (MERTK)\* (green), and anti-rhodopsin (Rho) antibodies (red); (b) is a confocal microscopy slicing of the selected area from (a). Nuclei are stained with DAPI. (c) A co-localization diagram (upper panel) and histogram (lower panel), showing the partial co-localization of anti-phospho MERTK\* and anti-Rho immunostaining. (d, e) Western blotting analysis of MERTK phosphorylation during the exposure of KGN cells to either POS (d) or apoptotic oocytes (e) with a graph representing

MERTK phosphorylation over time normalized to phospho-MERTK\* level at time 0; \*\*P < 0.001 by ANOVA test with Bonferroni post hoc analysis. **(f-h)** Immunostaining with anti-myosin II (Myo II) (green) and anti-Rho (red) antibodies **(f, g, h)** or with anti-Rho (red) antibodies **(f')**. **(g)** Is a 3D reconstruction of **(f)**. **(h)** A selected area from **(g)** showing the fine structure of Myo II clump containing the POS (double immunostaining, top panel), and after the omission of anti-Myo II (middle panel) and anti-Rho (bottom panel) immunostaining. Nuclei are stained with DAPI. **(i)** Co-localization diagram (upper panel) and histogram (lower panel), showing the partial co-localization of anti-Myo II and anti-Rho immunostaining..

**Figure 3** Uptake of apoptotic substrates but not of inert microspheres results in the lipidation of microtubule-associated protein 1 light chain 3 protein.

**(a, b)** IF pictures of the human granulosa KGN cells challenged with POS **(a)** and fluorescent microspheres/beads (red) **(b)**. Immunostaining with anti-Rho (red) **(a)** and with anti-light chain 3 (LC3) (green) **(a, b)** antibodies. Arrows in **(a, b, left panels)** denote LC3-labeled dots, asterisks (\*) in **a, (right panel)** mark co-localization sites of anti-LC3 and anti-Rho immunoreactivity. The nuclei are stained with DAPI. **(c)** Western blotting analysis of LC3-I and LC3-II protein content during exposure of KGN cells to fluorescent microspheres (beads) (upper panel), POS (upper panel and bottom panel, on the left), and apoptotic oocytes (bottom panel, on the right). Note the gradual decrease of housekeeping gene GAPDH during the incubation of cells with apoptotic substrates. MW: molecular weight markers. **(d)** Confocal picture of KGN cells challenged with POS after staining with anti-LC3 (green) and anti-Rho (red) antibodies. **(e)** A 3D reconstruction of **(d)**. **(f)** A selection from **(e)**, in which anti-LC3 (upper panel) or anti-Rho (lower panel) staining were omitted for better visualization of structures of interest. Confocal microscopy slicing **(d, right and lower panels)** denotes LC3-stained fragment of POS in cell cytoplasm (asterisk(\*)). Arrow shows nascent phagocytic cup co-stained with anti-LC3 antibodies. **(g)** A co-localization diagram (upper panel) and histogram (lower panel), showing

the partial co-localization of anti-LC3 and anti-Rho immunostaining. **(h)** Western blotting analysis of LC3-I and LC3-II protein content during exposure of KGN cells to POS with a graph representing the ratio of LC3-II/LC3-I over time;  $^{***}P < 0.001$  by ANOVA test with Bonferroni post hoc analysis. **(i, j)** KGN cells challenged with apoptotic oocytes, stained with anti-LC3 (red) and anti- zona pellucida glycoprotein 3 (ZP3) (green) antibodies. **(j)** Confocal microscopy slicing of the selected area from **(i)**. In **(j)** DAPI staining is omitted to better visualize the phagocytic cup at the surface of KGN cell, engulfing the fragment of an apoptotic oocyte (arrows) stained with anti ZP3-antibodies, and intracellular vacuole stained with anti-LC3 antibodies which shows very faint anti-ZP3 immunoreactivity (asterisk  $*$ ). **(k)** A 3D reconstruction of **(i)**. **(l)** Selection from **(k)**, with the omission of DAPI staining (upper panel) or DAPI and ZP3 (green) staining (lower panel) to better visualize the structure of the phagocytic cup (arrow) and phagosome (asterisk). **(m)** Western blotting analysis of LC3-I and LC3-II protein content during exposure of KGN cells to apoptotic oocytes with a graph representing the ratio of LC3-II/LC3-I over time;  $^{***}P < 0.001$  by ANOVA test with Bonferroni post hoc analysis.

**Figure 4** Ingestion of apoptotic oocytes by human GC engages autophagy proteins.

Confocal pictures of the human granulosa KGN cells **(a, b, e-h, j, k, n-q)** challenged with POS **(a, b, j, k)** or FITC-labeled **(e-h)** and unlabeled **(n-q)** oocytes. **(a, b)** Immunostaining with anti- autophagy related protein 5 (ATG5) (green) antibodies. Confocal section **(a)** and 3D reconstruction **(b)** show green-labeled phagocytic cup (arrow) on the surface of KGN cell co-stained with anti-Rho antibodies (red). Right panels in **(b)** are the selected area from the left panel, in which anti-ATG5 (upper panel) or anti-Rho (lower panel) staining were omitted for better visualization of structures of interest. Asterisk  $*$  denotes a small anti-ATG5-stained vesicle, co-stained with anti-Rho antibodies in cell cytoplasm. Nuclei are stained with DAPI. **(c)** A co-localization diagram (upper panel) and histogram (lower panel), showing the partial co-

1033 localization of anti-ATG5 and anti-Rho immunostaining. **(d)** Western blotting analysis of ATG5  
 1034 content during exposure of KGN cells to POS with a graph representing ATG5 content over  
 1035 time, normalized to ATG5 level at time 0, with no significant differences by ANOVA test with  
 1036 Bonferroni post hoc analysis. **(e-h)** KGN cells challenged with FITC-labeled apoptotic oocytes.  
 1037 Immunostaining with anti-ATG5 (red) antibodies. Note that the FITC-labeled fragment from the  
 1038 preparation of apoptotic oocytes is stained with DAPI (confocal microscopy slicing **(e, right**  
 1039 **panels)**). **(f)** A 3D reconstruction of the selected area from **(e)**, anti-ATG5 (red) or FITC (green)  
 1040 staining were omitted from **(g)** and **(h)** panels respectively. Asterisk (\*) denotes the intracellular  
 1041 fragment of FITC-labeled apoptotic oocyte (green), enclosed in a vacuole stained with anti-  
 1042 ATG5 antibodies (red). **(i)** Western blotting analysis of ATG5 content during exposure of KGN  
 1043 cells to apoptotic oocytes with a graph representing ATG5 content over time, normalized to  
 1044 ATG5 level at time 0; \*\*P < 0.001 by ANOVA test with Bonferroni post hoc analysis. **(j, k)**  
 1045 KGN cells challenged with POS. Immunostaining with anti-Becn1 (Bcn1) (green) antibody and  
 1046 anti-Rho (red) antibody. Confocal section **(j)** and 3D reconstruction **(k)** show phagocytic cup  
 1047 (arrow) on the surface of a KGN cell. Right panels in **(k)** are the selected area from the left  
 1048 panel, in which anti-Rho (upper panel) or anti-Bcn1 (lower panel) staining were omitted for  
 1049 better visualization of structures of interest. Nuclei are stained with DAPI. **(l)** A co-localization  
 1050 diagram (upper panel) and histogram (lower panel), showing the partial co-localization of anti-  
 1051 Bcn1 and anti-Rho immunostaining. **(m)** Western blotting analysis of Bcn1 content during  
 1052 exposure of KGN cells to POS with a graph representing Bcn1 content over time, normalized to  
 1053 Bcn1 level at time 0; with no significant differences by ANOVA test with Bonferroni post hoc  
 1054 analysis. **(n-q)** KGN cells challenged with apoptotic oocytes. Immunostaining with anti-Bcn1  
 1055 (red) and anti-ZP3 (green) antibodies. **(o)** A 3D reconstruction of the selection from **(n)**. In **(p, q)**  
 1056 anti-Bcn1 **(p)** and anti-ZP3 **(q)** staining were omitted for better visualization of structures of  
 1057 interest. Asterisk (\*) denotes a fragment of apoptotic oocyte, labeled by anti-ZP3 antibody  
 1058 (green), enclosed in a vacuole stained with anti-Bcn1 antibodies (red). **(r)** Western blotting

analysis of Bcn1 content during exposure of KGN cells to apoptotic oocytes with a graph representing Bcn1 content over time, normalized to Bcn1 level at time 0, with no significant differences by ANOVA test with Bonferroni post hoc analysis. **(s, t)** Phagocytosis by KGN cells after rapamycin treatment. **(s)** IF pictures of control (upper panels) and rapamycin-treated (lower panels) KGN cells after 2 h exposure to POS. Immunostaining with anti-Rho (red) and anti-LC3 (green) antibodies. Arrows indicate the small fragments of POS. Asterisks (\*) denote the large fragments of POS, associated with the plasma membrane of KGN cells. **(t)** Depicts a quantitative analysis of bound and total (bound + ingested) POS associated with KGN cells. Left histogram: phagocytosis index for control KGN cell cultures challenged with POS. Right histogram: phagocytosis index for KGN cell cultures pretreated with 200 nM rapamycin for 24 h.  $**P < 0.001$  by ANOVA with Bonferroni post-hoc analysis.

**Figure 5** Degradation of ingested apoptotic substrates by human GC requires lysosomal proteolysis.

Gomori staining **(a, b, c)** for acid phosphatase (brown dots) in control GC **(a, black arrows)** and after incubation with apoptotic oocytes **(b)** and POS **(c)**. In **(b, c)** black arrows denote Gomori staining in cell periphery, white arrows denote brown dots encircling plasma membrane, white asterisks (\*) denote Gomori staining next to cell nucleus. **(d, upper panel)** Histogram showing the total area of brown dots/per cell during phagocytosis of apoptotic oocytes and POS.  $**P < 0.001$  by ANOVA test with Bonferroni post hoc analysis. Confocal pictures **(e, i, j)** and 3D reconstructions **(f, g, h, k)** of the human granulosa KGN cells challenged with POS **(e-h)** or with the fragments of apoptotic oocytes **(i-k)**. **(e-h)** Immunostaining with anti-Cathepsin D (CatD) antibodies (green) at different times of incubation (2 **(e, f)**, 4 **(g)**, 6 **(h)** hours) with POS (anti-Rho immunostaining (red)). **(f)** A 3D reconstruction of **(e)**. Note the vesicular pattern of anti-CatD immunostaining. Nuclei are stained with DAPI. **(d, lower panel)**

Histogram showing the total area of vesicles stained with anti-CatD antibodies/per cell nuclei during phagocytosis of POS.  $**P < 0.001$  by ANOVA test with Bonferroni post hoc analysis. **(i, j, k)** Confocal pictures and 3D reconstruction **(k)** of KGN cells challenged with the fragments of apoptotic oocytes. Ocher is immunostaining with anti-CatD antibodies; green is immunostaining with anti-ZP3 antibodies. **(j)** Omission of anti-CatD immunostaining to better visualize the fragments of DAPI-stained apoptotic oocytes bound to- **(1,3)** and ingested by **(2, 4)** KGN cell as shown by confocal slicing **(i-k, lower panels)**. **(l)** Western blotting analysis of CatD protein content during exposure of KGN cells to POS (left) or to apoptotic oocytes (right) with a graph representing CatD content over time, normalized to CatD content at time 0.  $**P < 0.001$  by ANOVA test with Bonferroni post hoc analysis. **(m, n, o)** Electron micrographs of control KGN cells **(m)** and cells challenged with the fragments of apoptotic oocytes **(n, arrow)** or POS **(o, arrow)**. Note the accumulation of lysosomes (ly) in the cytoplasm of cells in **(n)** and **(o)**. **(p)** Quantification histogram of lysosome content/per nucleus in control KGN cells, and after exposure to apoptotic oocytes and POS. **(q, r)** Western blotting analysis of sequestosome 1/p62 (p62) protein content during exposure of KGN cells to POS **(q)** and to apoptotic oocytes **(r)** with a graph representing p62 content over time, normalized to p62 content at time 0; with no significant differences by ANOVA test with Bonferroni post hoc analysis.

**Supplementary Figure S1** Interaction of human granulosa KGN cell line with apoptotic substrates,

**(a)** Immunofluorescent pictures of the cultured human granulosa KGN cell line incubated with the fragments of photoreceptor outer segments (POS), revealed with antibodies against rhodopsin (Rho) (red). Right panel in **(a)** is the merge of left panel with DIC projection to

better visualize cell shapes. Note the POS in cell periphery (arrow) and close to the nucleus stained with 4', 6 diamidino-2-phenylindole (DAPI) (arrowhead).

**(b)** Confocal pictures of the cultured granulosa KGN cell line incubated with 1  $\mu$ m inert microspheres/beads (green) and stained with anti-autophagy related protein 5 (ATG5) antibody (red) (left panel). In central and right panels red or green staining were omitted to better visualize the absence of co-localization.

**(c)** Confocal pictures of the cultured granulosa KGN cell line incubated with 1  $\mu$ m inert microspheres/beads (green) and stained with anti-Becn1 (Bcn1) antibody (red) (leftpanel). In central and right panels red or green staining were omitted to better visualize the absence of co-localization.

**(d)** Western blotting (WB) analysis of the content of autophagy related protein 7 (ATG7) in the lysates of KGN cells during the incubation (hours) with apoptotic oocytes (left panel), or POS (right panel) with the graphs representing ATG7 content over time, normalized to ATG7 level at time 0; with no significant differences by ANOVA test with Bonferroni post hoc analysis. MW: molecular weight markers.

**(e)** Western blotting analysis of the content of microtubule-associated protein 1 light chain 3 (LC3) protein in the lysates of KGN cells after 24 h treatment with 200 nm rapamycin (upper panel); lower panel – the content of glyceraldehyde-3-phosphate dehydrogenase (GAPDH) in the same lysates.

**(f)** WB analysis of Cathepsin D (CatD) content in the lysates of human retinal pigment epithelial hTERT-RPE1 cells challenged with POS. Note the strong band around 50 kDa corresponding to proCatD.

1132

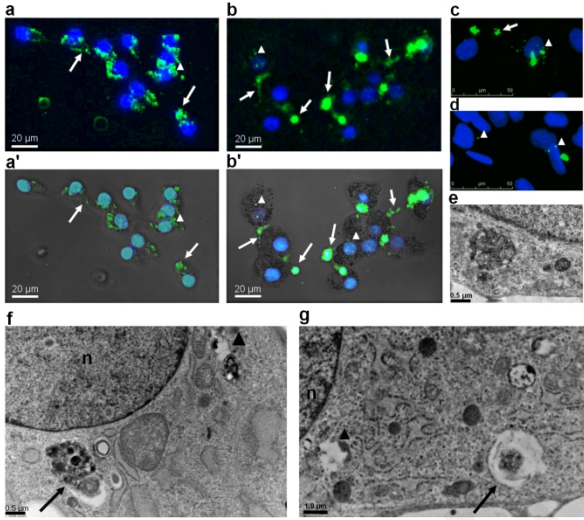


Fig.1

209x297mm (300 x 300 DPI)



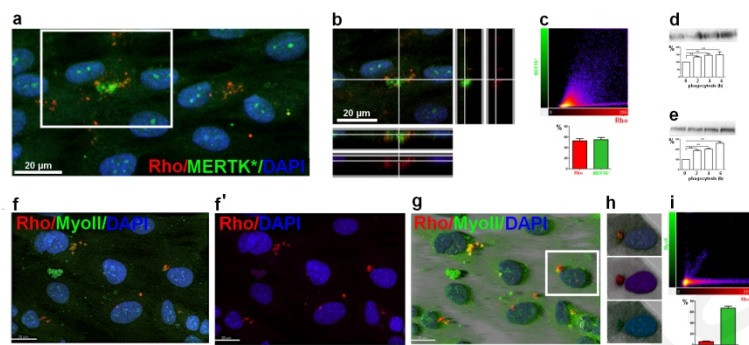


Fig.2

209x297mm (300 x 300 DPI)

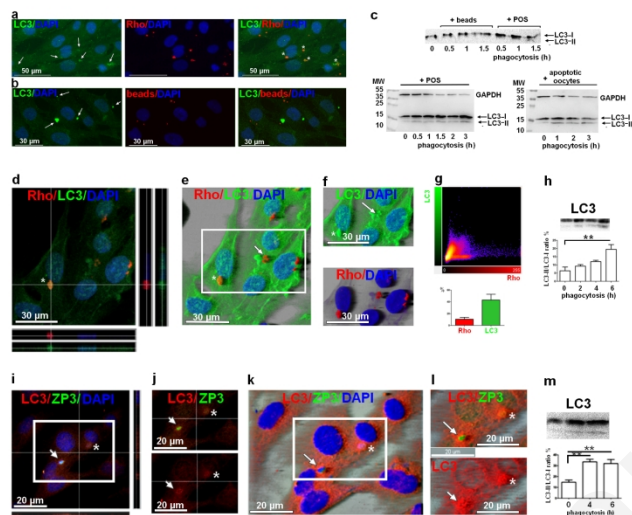


Fig.3

209x297mm (300 x 300 DPI)

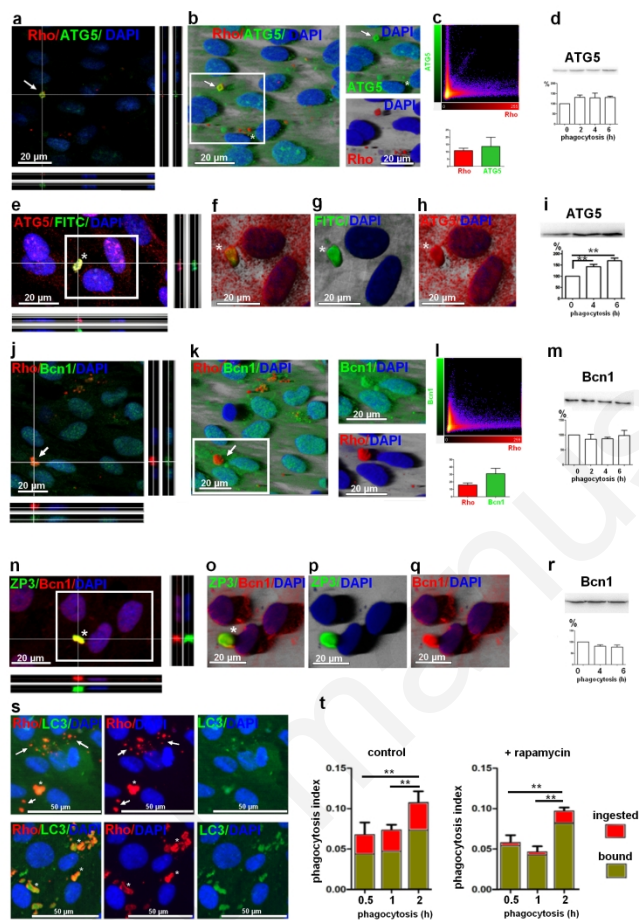


Fig.4

209x297mm (300 x 300 DPI)

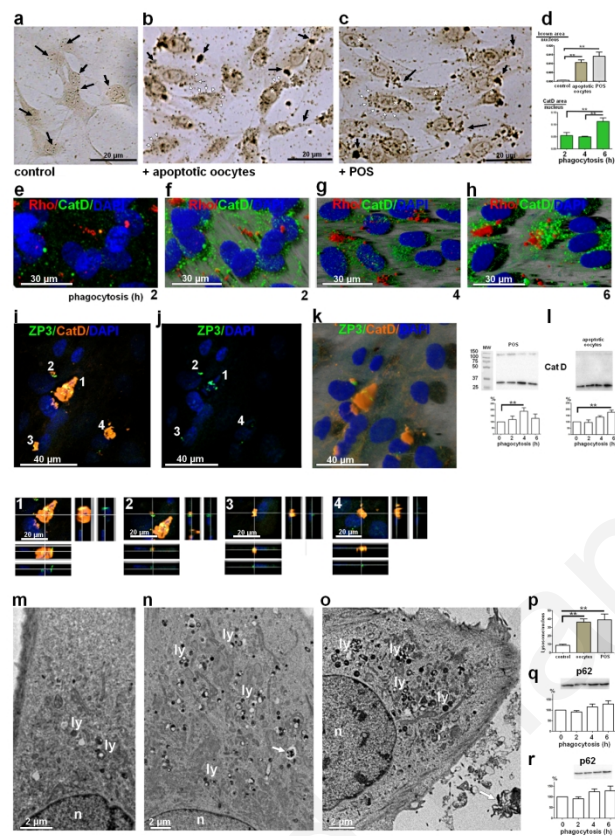
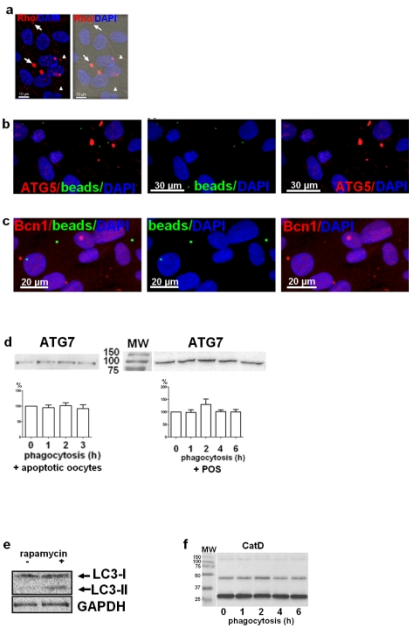


Fig.5

656x928mm (96 x 96 DPI)



Supplementary Fig.1

209x297mm (300 x 300 DPI)